DOI: 10.1002/cphc.200((will be filled in by the editorial staff))

Direct Observation of the Electroadsorptive Effect on Ultra Thin Films for Microsensor and Catalytic Surface Control

Theodor Doll*[a], Juan J. Velasco-Velez[a,b], Dirk Rosenthal*[c], Jonathan Avila[d,e] and Victor Fuenzalida[e]

((Dedication, optional))

Microchemical sensors and catalytic reactors make use of gases during adsorption in specific ways on selected materials. Fine tuning is normally achieved by morphological control and material doping. The latter relates surface properties to the electronic structure of the bulk, which suggest the possibility of electronic control: Whilst being unusual for catalytic surfaces such phenomena were reported for microsensors at times, however with little understanding of the underlying mechanisms.

Here we report the direct observation of the electroadsorptive effect by combined XPS and conductivity analysis on nm- thin semiconductor films on buried control electrodes. For the SnO_2 / NO_2 model system we find that the formation of NO_3 surface species, which normally decay at the latest within minutes, can be kept stable for 1.5 hrs with high coverage of 15% under appropriate electric fields. This includes uncharged states too and implies that nanoelectronic structures provide control over predominant adsorbate conformation on exterior surfaces which opens the field for in-situ tunable chemically reactive interfaces.

Introduction

The effect of electric control on gas adsorption at surfaces was postulated as early as the invention of semiconductor devices when the effort spent on electronics development dealt a lot with surface and interface states. In parallel, catalysis made tremendous use of the latter, however the interplay between electronic states on one side and geometrical effects on the other and chemical reactivity seemed to be an unsolved puzzle: A direct examination, of either the geometric or the electronic effect was lacking. We present a first combination of semiconductor sensor measurements coupled with surface analysis on a model system under the dominating electronic effect of electronic surface states control. The results shine light on the molecule-surface interactions, which fit well into an interdisciplinary view using semiconductor device physics, surface analytical techniques and theory of catalysis.

The story turns back to 1930, when Lilienfeld patented a semiconductor structure that laid the basis for later field effect transistors (FET) [1]. The patent postulated the conductivity control of a thin semiconductor layer by means of an external electric field. In 1935 Heil presented a suspended gate structure that should control surface states and hence the conductivity of a thin film by external electric fields, too [2]. The malfunction of these early structures kept to be unexplained until in 1948 Shockley and Pearson could clarify that only 10 % of the charge carriers in such thin film arrangements were mobile [3]: Surface and interface states dominated all device behaviour. The effort spent on diminishing and saturating interface defects for MOS technology since the mid of the 1950ies is unparalleled and aid was seeked from all neighbouring disciplines. In turn interdisciplinary insights arose in the manipulation of adsorbed species and their use for gas detection by later developed semiconductor sensors and also in catalysis. For the latter, chemical view, the first quantum mechanical description of coupled solid interface – adsorbate systems was given by Wolkenstein [4], who, in 1958, presented a theory on the influence of electric fields on adsorption and desorption, named the “Electroadsorptive Effect” (EAE) [5].

The effect was experimentally observed e.g. by Keier in 1964

[a] *Prof. Dr. T.Doll*
Microstructure Physics
University of Mainz
Staudinger Weg 7, 55128 Mainz, Germany
E-mail: dollth@uni-mainz.de

[b] *Dr. J.J. Velasco-Velez*
Materials Science Division
Lawrence Berkeley National Laboratory
Cyclotron Road, Berkeley CA 94720, USA

[c] *Dr. D. Rosenthal*
Inorganic Chemistry
Fritz-Haber-Institut der Max-Planck-Gesellschaft
Faradayweg 4-6, 14195 Berlin, Germany
E-mail: dirkrose@fhi-berlin.mpg.de

[d] *Dr. J. Avila*
Laboratorio de Filmes Finos e Superficies (LFFS), CFM
Universidade Federal de Santa Catarina
Caixa Postal 476, CEP 88040-900 Florianópolis, SC, Brasil

[e] *Prof. Dr. V. Fuenzalida*
Departamento de Física
Universidad de Chile
Av. Blanco Encalada 2008, Santiago – Chile

Supporting information for this article is available on the WWW under http://www.chemphyschem.org or from the author.

with methanol on germanium [6] or Hoenig, who found for O_2 on ZnO [7] clear in- and decreases in adsorption-induced thin film conductivities under electric fields as strong as 36 kV/cm. As such fields are too close to the normal discharge limit in air, a practical use seemed to be chanceless.

Also, in the 1970ies, catalysis looked on the EAE as it was found that semiconductor doping levels could not influence apparent activation energy levels. Ertl and Gerischer pointed out that field effects could still enhance reactivities if charged adsorbates were more reactive than uncharged ("weak") ones [8]. However, any studies were hampered by surface impurities at this time. In turn, morphological aspects evolved as the prevailing paradigm of the field.

For the electronics site, conditions changed with the up come of micro- and nanotechnological devices in which, at one hand, several volts dropping across few or tens of nanometres show that today insulators can bear extreme electric strengths. At the other hand semiconducting thin films for chemical sensing got available with largely improved purities. Hence, since the 1990ies the EAE and Wolkenstein's theory got revived by several semiconductor gas microsensors findings [9-14] and later, in nanosensing [15, 16].

Nevertheless the detailed mechanisms that govern surface reactions in the presence of external electric fields remained not entirely understood. Also details on the surface states involved are sparse as most observations stem from indirect measurements.

In this study we add direct surface analysis to semiconductor measurements. For the material, we chose tin oxide layers as they come with vast knowledge for their semiconductor sensing properties [17, 18]. Similar reasons suggest the use of NO_2 for test reactions [19 - 23]. With high electric fields added during and after exposure a chemical analysis of adsorbates as well as a characterization of the underlying semiconductor is performed and both measurements are discussed on the basis of an extended Wolkenstein modelling.

Results and Discussion

XPS Measurements

XPS analysis was started a few minutes after exposing compact or porous SnO_2 layers towards NO_2 /O_2 mixtures. The analysis of the N1s photoelectron signal shows peaks at 406 eV and 408 eV binding energy related to chemisorbed NO_2 and NO_3 respectively [23 - 25]. On the other hand peaks at 400 eV and 399 eV are associated to Sn-NO_{ad} and nitrogen replacing the oxygen in the crystal lattice [26 - 28]. The latter peaks around 400 eV appear after NO_2 exposure on freshly prepared films and remain stable for days in contrast to the peaks of NO_2 and NO_3.

As both the compact and the porous layers show very similar adsorption characteristics (besides the total amount of adsorbed gas and its desorption over time, see experimental), the average from a series of 70 measurements has been calculated and is presented as a schematic reconstruction of the porous and the compact layers in figure 1. For zero voltage (see supplemental), we find NO/N to be the dominating stable species with partial coverages 54%. Both NO_2 and NO_3, which start at approx. 28 % resp. 18 % coverage, fade away during our 90 min period of observation with 40 min (porous) and 25 min (compact) decay time.

Figure 1 gives the averaged N1s photoelectron signals as a function of time for positive and negative polarization. Figure 1(a) shows that under the application of positive potentials (negative electric fields) the NO_2 peak reaches 80 % of the signal height of the NO/N species and decays much slower over time. The NO_3 species get only slightly pronounced, however their stability over time is clearly enhanced. In total we find a stabilization and intensification of the NO_2/NO_3 configuration under positive potentials.

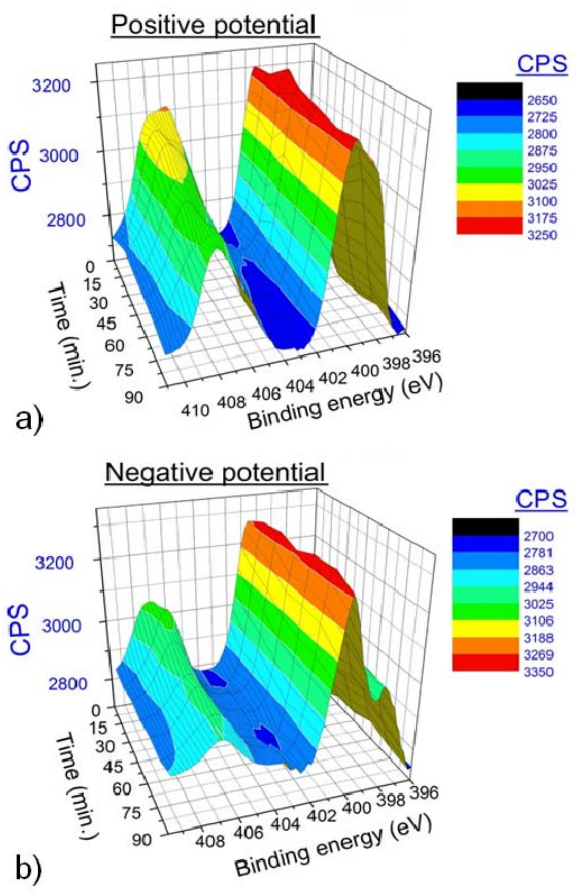

Figure 1. Schematic reconstruction of the XPS-results of the porous and compact layer results: N1s-peak (400 eV binding energy) development over time under positive (a) and negative (b) bias. The peaks arising at 406 and 408 eV correspond to NO_2 and NO_3, respectively.

On the other hand, the application of a negative potential (positive electric fields) stimulates the desorption of NO_2 and NO_3 from the SnO_2 surface as seen from Figure 1(b). NO_3 is almost entirely missing after the short transfer period. NO_2 starts at similar values like under zero voltage (50 % relative peak height) decays more quickly. In addition to that, we find an increase of the NO/N peak over time for the porous layer (see supplemental) that clearly surmounts porosity effects discussed below.

Changes may partially arise from bias-dependant inner-diffusion of interstitial nitrogen species inside the bulk by means of a driving force (electric field). The application of a positive voltage induces the accumulation of Sn-N states at the surface. Vice versa, the negative potential produces a diffusion of N towards inside the bulk reducing the concentration at the surface. This is affirmed by other studies based on angle-

resolved XPS (AR-XPS) which provides surface and bulk (thickness <6 nm) chemical information [29].
The finding provides explicit evidence on the electric desorption control of chemisorbed species. As a general trend the pronounced desorption under negative potentials comes in parallel with some increase of lattice nitrogen (i.e. Sn-O-N) which is higher for the rougher evaporated thin films. In contrast, under positive voltages, desorption is strongly suppressed. The same conclusion is supported by reassessing the N1s intensities with respect to C1s.

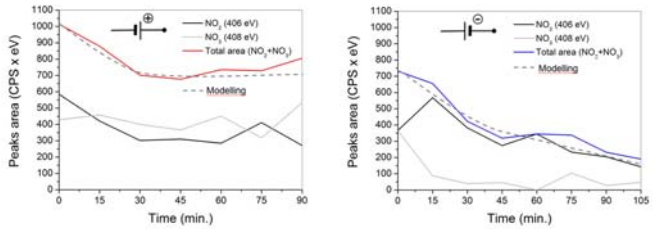

Figure 2. Time dependence of peak areas (porous sample) of NO_2 (406 eV) and NO_3 (408 eV) under polarization at positive voltage (left) and negative voltage (right). The red/blue lines are the total peak area (NO_2 and NO_3). The dotted line reflects our modelling results.

The energy split between the NO_2 (406eV) and NO_3 (408 eV) is wide enough to identify both species univocally. The peak area measurements of both single components can be seen in Figure 2 which shows that the applied voltage drastically affects the desorption of the NO_3 species. Positive polarization suppresses desorption during the period under study, whilst negative polarization causes rapid desorption of NO_3 in comparison to NO_2.
Beneath desorption another process is very likely to happen: The increase in either NO (or N) species amounts to 6% peak height according to Figure 1 for negative voltages. As surface-N undergoes bulk diffusion, it must originate from a conformational change of other adsorbed species. They may be NO_3 (or NO_2), which are seen from Figure 2 to drop at least by 30% even in the positive case. The XPS intensities show that about 20% of NO_3 (or NO_2) get transformed whilst the remaining are lost by desorption.

Conductivity measurements

The electrode configurations on our test devices allow for simultaneous read out of the field effect inside the semiconductor thin film. Herein pure voltage depending electronic processes get superimposed by gas sensitive effects that are non-linearly depending on the amount of adsorbed species. Their surface states can be charged according to the adsorption- modified surface statistics which in turn is ruled by the bulk Fermi level.
The change in conductivity due to adsorbed gases is related to the formation of a space charge region adjacent to the surface. The biasing electric field produces a second space charge region that arises at the buried insulator-semiconductor interface (see inset of Figure 3). An appropriate biasing field will control both the device conductivity and the adsorption/de-sorption at the metal-oxide surface. It is worth noticing that for enabling the electric field to reach the surface the space charge region must cross the whole semiconductor thickness whilst for measurable conductivity one path parallel to the surface must remain at the same time.
Figure 3 shows the conductivities recorded during the XPS experiment. According to normal transistor operation (-30…-22,5 min) we find a higher current under positive voltages which means that the backward end of the space charge is diminished and the conducting path is widened. The effect of negative voltages runs vice versa.
For gas exposure to NO_2 a general decrease in conductivity fits to the oxidative nature of NO_2, formation of NO_x^- acceptor surface states, widening of the space charge region and, as a result, a narrowed conductive path. The time constants agree well with other findings for room temperature metal oxides [30]. The response under biasing voltage differs both in absolute and relative measures: Whilst the absolute values are relevant for catalysis, as the total number of ionized adsorbates is changed, the relative changes count for sensor applications. For positive voltages the absolute (relative) change amounts to 1,35 a.u. (10). For negative bias 0,67 a.u. (6) is yield. For the decay back to the baselines we find also a faster desorption for negative bias voltages consistently to XPS intensities.

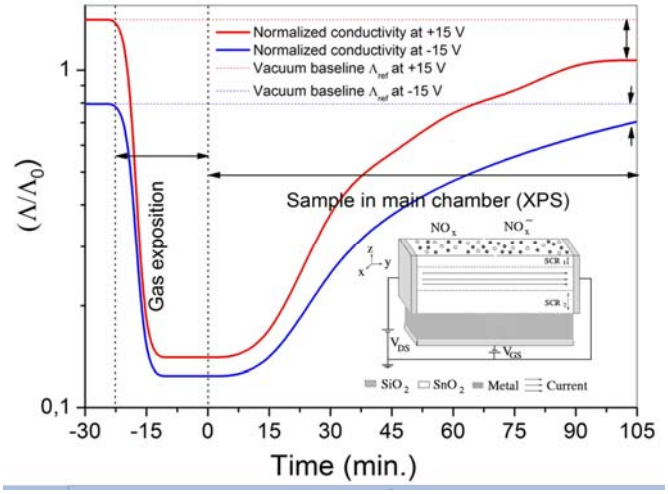

Figure 3. Conductivity (porous sample) related to the NO_x presence at positive voltage application (+15 V) and at negative potential (-15 V). Point lines show the reference conductivity in absence of gases (baselines). Inset: Thin film transistor device model.

Conclusion

The surface species for NO_2 adsorption in SnO_2 are consistent with Maiti's findings [23] which are extended towards their control under electric fields. We observe a strong dependence of adsorption/desorption for NO_3 species on electric fields with almost On/Off characteristics. In general one can assume that both NO_2 and NO_3 states may be present in charged and uncharged states at the surface, which both are under control of the electric field. As, due to the Weisz limit [31], the 30% increase observed cannot stem from all charged species, we conclude that also uncharged states are controlled by the electric field. If the Wolkenstein model is combined with the appropriate Shockley-Read-Hall statistics and literature parameters are used, also the dynamic behaviour of the coverages of the latter species can be well described as is depicted in Fig.2 (dotted line). We find that the electroadsorptive effect influences the total amount of adsorbed NO_x: Its coverage gets enhanced under positive

voltages and adsorbates stays longer there. Thus for surface reactions more NO_x is available, and especially, if a desired reaction would necessitate the NO_3 conformation, the EAE can promote such reactions. Even more important is the fact that two different (polycrystalline) surface morphologies yield similar results. Thus the EAE offers a vital approach for catalytic surface optimization independent from morphological strategies.

With regard to semiconductor sensor applications we find that the potential for using the EAE is more limited. This is due to the fact that only charged adsorbates are directly observed under electronic readout. However counteractions with other adsorbates may play important roles also. The role of coadsorbed oxygen and water remainders are still not considered and existing onsets [32] of a multi- surface state modelling will need substantial data.

Some approach towards them would be in situ experiments, e.g. by AP-XPS and XAS. The first offers the opportunity to reach pressure in the range of several ten Torr which is enough for our requirements. On the other hand, secondary electrons collected in the sensitive layer may provide information on the interface between solid and gas under ambient pressure conditions. Such measurements are planned in a high pressure gas cell with mixtures of various gases.

Experimental Section

Device

A sensor-like semiconductor nanofilm setup was designed for direct observation of the EAE by X-ray photoelectron spectroscopy (XPS). For high field strengths and the bare surfaces needed, a buried control electrode underneath the layer was chosen. Thus the device is similar to a film transistor. By using layer thicknesses in the range of several Debye lengths L_D [33] it is ensured that the rear electric field penetrates the entire layer and reaches the front surface. For the sensitive metal oxide layer we chose SnO_2 with, in our case, L_Ds is of approx. 40 nanometres at room temperature. NO_2 was selected as adsorbing model gas due to the vast amount of data reported on the NO_2 / SnO_2 system.

The device is shown in Figure 4: For the back (buried) electrode a silicon n+ chip is used with silicon oxide as insulating layer towards the frontal thin SnO_2 layer. Small silver or gold lines at the rim of the SnO_2 serve for (a) electric grounding of the surface and (b) conductivity measurement on the layer. Also shown are the band diagrams for two states of operation: positive or negative back electrode voltage. For positive voltages, the electron energy of the electrode is lowered with a resulting electric field tilting the insulator bands upwards. The bands of the semiconductor layer are not tilted due to occurring Fermi level pinning for thicknesses in the L_D range. However, the Fermi level gets shifted upwards and extra negative charge is raised. This touches the surface states, too, which find themselves increasingly charged, as they are acceptor-type in our case. For negative backside voltages the scheme runs vice versa and the uncharged surface states prevail.

As in details, we see that the buried electrode potential determines the position of the Fermi level (E_F), which governs the surface state statistics and hence, the reaction probability. It is important to remind that, if only one adsorbed species is present, the main effect of the electric field is to alter the charging probability of adsorbates which is at ambient conditions below one per cent ("Weisz"-self limitation [31]). However, if competitive adsorption of several gases is involved, the final result will depend on the availability of free adsorption sites and hence the several binding strengths and partial gas pressures.

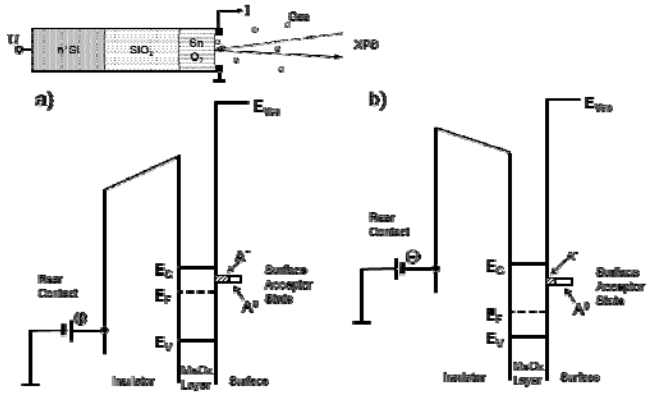

Figure 4. Theory of adsorption behavior of the back electrode insulator semiconductor structure: (a) positive potential induces adsorption of charged species (A^-), A^0 is referred to neutral species (not charged). (b) negative potential induces its desorption.

According to frequent discussions we want to clarify that due to the presence of electronically vacant surface states no electric field leaves the frontal surface. As its rim has been electrically tied to ground, no charging effects superimpose to the XPS measurements. This has been carefully cross-checked with C1s calibration and the other O1s and Sn3d peaks. Thus, the entire surface band structure was grounded which includes core levels, too. The surface states can either fade away in terms of existence (no adsorbed molecule in a specific conformation= no state), or their electronic occupation statistics can be changed by the Fermi Level, which is altered by the backward field. Additionally, if one adsorbed molecule is able to change its conformation (This is our case where NO can, by eating adjacent atoms, transform itself into the states NO_2 and NO_3), one surface state disappears and reappears at another position within the band gap.

What is observed in XPS are field-depending chemical shifts on a quasi neutral background, as the probing depth of XPS is much smaller then the space charge region width.

The SnO_2 layer deposition was performed either by Ar/O_2 RF sputtering from a SnO_2 target followed by annealing in dry synthetic air (400°C / 100 hrs) or by e-beam evaporation from pure Sn with humid air oxidation (400°C / 24hrs). The resulting oxide layers were 100 nm thick and had an intrinsic doping level of approx. 10^{18} cm^{-3} oxygen vacancy concentrations according to measurements on identically prepared layers [34]. The insulator thickness varied from 1 µm (sputter) to 100 nm (e-beam). A transmission electron micrograph (TEM) investigation on the sputtered structures showed that the devices had compact layers with crystallite domains ranging from 5 to 25 nm and missing texture and surface faceting (see Figure 5). Thus gas diffusion along grain boundaries of the sputtered samples is rather unlikely. The layer can be considered as amorphous in terms of X-ray analysis. The evaporated samples, however, came with high surface roughness and a thickness ranging from 20 nm to 100 nm. The EDX analysis showed a stoichiometry that was sufficient for a doping concentration ensuring the Debye criteria for the functioning of the effect.

Two mayor differences between porous and compact layers have been observed: At first, the XPS Sn-N lattice peak was by far more prominent in the evaporated samples which may be due to residual gas pressures of 5E-6 mbar during deposition. Secondly, the porous samples showed slightly increasing surface coverages during analysis (up to 6% over time), whilst the compact layers had (normal) overall decays. The increases were found to be voltage-insensitive and have been attributed to a relocation of adsorbed species from pores and grain boundaries.

By combining both porous and compact layer data these differences get suppressed and the pure EAE effect is highlighted.

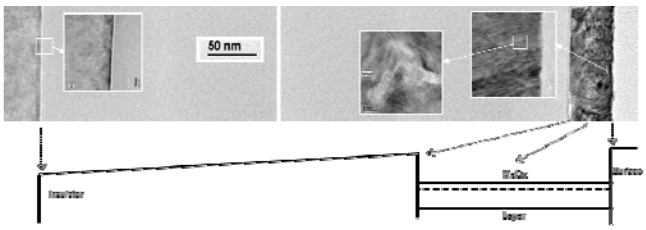

Figure 5. TEM cross section of the entire device structure. Buried silicon electrode (left), Si_3N_4 insulator (140 nm / 250 nm) and SnO_2 sensing layer (right). The high resolution sensing layers shows the compact structure and approximate grain size of 5- 25 nm. No preferential orientation is present.

Gas Exposure

A vacuum setup with a separate gas exposure chamber connected via sample transfer to the XPS measurement chamber was used, allowing continuous electrical control during manipulation. A NO_2/O_2 mixture (80/20 %) was internally produced by heating lead nitrate under mass spectrometry surveillance. The devices, stored under UHV, were exposed for 10 minutes at 10^{-3} mbar. Within 3 minutes after restart of HV pumping the devices were pushed into the main UHV chamber and the XPS time series was started. No measurements for t=0 are therefore available and quick desorbing species are excluded from observation. We note that in high vacuum systems the previously adsorbed molecules will, in first approximation, the longer stay at the surface the stronger their binding is. Beneath pre-/coadsorbed oxygen and water remainders NO-, NO_2- and NO_3-species (all: "NO_x") as well as interstitial nitrogen can be identified by XPS regardless of their possible charging. Following Rodriguez's results on TiO_2 [24] we expect that chemisorbed NO_2 will either decompose to give NO_{ad} and O_{ad} or disproportionate to give NO_3 and NO. Figure 6 depicts the preferred sites of these adsorbates on the (110) SnO_2 surface plane which is the most common facet in polycrystalline surfaces [17] within quasi-amorphous blurring of defects.

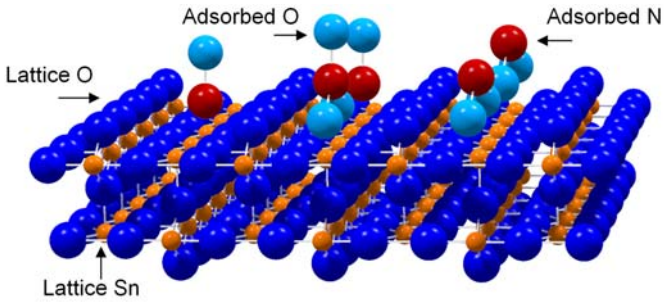

Figure 6. Most common SnO_2 (110) surface after adsorption of NO_2 from the gas phase with NO, NO_2 and NO_3 species. Lattice oxygen and tin as well as O and N in adsorbed species are marked by arrows.

Modelling

The Wolkenstein-Geistlinger model [4, 5, 35, 36] formulates a Fermi-level dependent adsorption coefficient ß that is multiplied by the partial pressure in a standard Langmuir isotherm. The model takes into account the quantum-chemistry of chemisorption wherein physisorption is considered as an independent precursor of two chemisorbed states ("strong" and "weak"). In this view the "weak" state remains uncharged and, in terms of charging, is not different from the physisorbed state that, however, has a different (i.e. smaller) binding energy. Both, "weak" and "strong", are governed by the Fermi level. As the position of the surface states is referenced to the vacuum level, both states are sensitive to electric field via the surface band bending ΔV_S but only the charged ones are electrically detected: With two space charge regions (*b*ulk and *f*ront), the electrical conductance G can be described as $G= \sigma_0(W/L)(d\text{-}SCR_b\text{-}SCR_f)$ with W/L geometric parameters (width and length respectively), σ_0 as bulk conductivity, d giving the layer thickness and SCRs denoting the space charge region depths. SCR_b is purely electronic and SCR_f gas sensitive and electronically influenced. For the sought dynamic response the Wolkenstein isotherm was combined with Shockley-Read-Hall statistics [31, 32, 37] that describes the temporal fluctuations of charged adsorption by means of capture processes. For example, the desorption of charged, "strong" chemisorbed adsorbates is described by a capture coefficient K_n that rules over the remaining "weakly" adsorbed ones $N^0 = (N - N^-)$ with electron transitions from the surface conduction band E_{CS} and desorption from the adsorption levels described as trap states E_t.

$$\frac{dN^-}{dt} = K_n[(N-N^-)N_c exp[-\frac{E_{cs}-E_F}{kT}] - N^- N_c exp[-\frac{E_{cs}-E_t}{kT}]].$$

The results of such modelling [38] are shown as a segmented line in Figure 2 exhibiting fair agreement of observed time- and voltage-dependence with modelling of the total sum of weak and strong chemisorbed NO_x^0 and NO_x^- particles. The time constants of XPS as well as conductivity measurement and modelling lie within the same range. This indicates that the charged molecules are present as a constant portion of the entire adsorbates or, to put it the other way around, the electric field governs the uncharged, "weak" states just in the same manner. That, in addition, the total sum of adsorbed nitrogen is controlled by the voltage, however, exceeds such modelling.

Acknowledgements

Partial funding of this work by DAAD/CONICYT ALECHILE 507357 and Grant FONDECYT 1110168 of the Chilean government is acknowledged. The authors gratefully acknowledge layer preparation (dev.1) by FhG IPM, Freiburg, Germany

Keywords: (electroadsorptive effect · catalysis · Wolkenstein theory · sensor · adsorption)

[1] J.S.E. Lilienfeld, US Patent 1, 745, 175, **1930**.
[2] O. Heil, British Patent No. 439457, **1934**
[3] W. Shockley, G.L. Pearson, *Phys. Rev.* **1948**, *74*, 232-233.
[4] T. Wolkenstein, *The Electron Theory of Catalysis on Semiconductors* Pergamon Press, Oxford, **1963** (translated, revised version from Russian original)
[5] F.F. Wolkenstein, W.B. Sandomirski, *Dokl. Acad. Nauk. SSSR*, **1958**, *118*, 980-982.
[6] E.P. Mikheeva, N.P. Keier, *Kinet. Katal.*, **1964**, *5*, 748.
[7] S.A. Hönig, J.R. Lane, *Surf. Sci.* **1968**, *11,* 163-174.
[8] G. Ertl, H. Gerischer in: Physical Chemistry, Vol. X, W. Jost (ed), Academic Press 1970
[9] L.I. Popova, S.K. Andreev, B.K. Guoerguiev, N.D. Stoyanov, *Sens. Act. B*, **1994**, *18/19,* 543-545.
[10] W. Hellmich, G. Müller, C. Bosch-von Braunmühl, T. Doll , I. Eisele, *Sens. Actuators B* **1997**, *43*, 132-139.
[11] M. Hausner, J. Zacheja, J. Gerblinger, J. Binder, German Patent DE 4442396 A1, **1996**.
[12] U. Storm, O. Bartels, J. Binder, *Sens. Act. B* **2001**, *77*, 529-533.
[13] M. Jaegle, J. Wöllenstein, T. Meisinger, H. Böttner, G. Müller, T. Becker, C. Bosch-von Braunmühl, *Sens. Act. B,* 1999, *57,* 130-134.

[14] M.S. Arnold, P. Avouris, Z.W. Pan, Z.L. Wang, *J. Phys. Chem. B*, **2003**, *107*, 659-663.
[15] Z.Y. Fan, J.G. Lu, *Appl. Phys. Let.* **2005**, *86,* 123510.
[16] P. Andrei, L.L. Fields, J.P. Zheng, Y. Cheng, P. Xiong, *Sens. Act. B*, **2007**, 128, 226-234.
[17] M. Batzill, U. Diebold, *Prog..Surf. Sci*. **2005,** *79*, 47-154.
[18] A. Gurlo, *Chem. Phys. Chem*., **2006**, *7*, 2041-2052.
[19] M. Epifani, J.D. Prades, E. Comini, E. Pellicer, M. Avella, P. Siciliano, G. Faglia, A. Cirera, R. Scotti, F.F. Morazzoni, J.R. Morante, *J. Phys. Chem*. *C*, **2008**, *112*, 19540-19546.
[20] A. Karthigeyan, R.P. Gupta, M. Burgmair, S.K. Sharman, I. Eisele, *Sens. Act. B* **2002**, *87*, 321-330.
[21] M. Law, H. Kind, B. Messer, F. Kim, P. Yang, Angew. Chem. Int. Ed. **2002**, *41*, 2405-2408
[22] T. Yoshida, N. Ogawa, T. Takahashi, *J. Electrochem. Soc.*, **1999**, *146*, 1106-1110 and references therein
[23] A. Maiti, JA. Rodriguez, M. Law, P. Kung, JR. McKinney, P. Yang, *Nano Lett.*, **2003**, *3*, 1025-1028
[24] J.A. Rodriguez, T. Jirsak, G. Liu, J. Hrbek, J. Dvorak, A. Maiti, *J. Am. Chem. Soc.*, **2001**, *123*, 9597-9605.
[25] J.A. Rodriguez, T. Jirsak, J.K. Kim, J.Z. Larese, A. Maiti, *Chem. Phys. Let*., **2000**, *330*, 475-483.
[26] S.S. Pan, C. Ye, X.M. Teng, H.T. Fan, G.H. Li, *Appl. Phys. A*, **2006**, *85*, 21-24.
[27] M. Xing, J. Zhang, F. Chen, *Appl. Catalysis B: Environmental*, **2009**, *89,* 563-569.
[28] Z. Zhai, K. Zou, W. Feng, Q. Wang, *Modern Applied Science*, **2010**, *4*, 95-100.
[29] K. Takasaki, K. Irino, T. Aoyama, Y. Momiyama, T. Nakanishi, Y. Tamura, T. Ito *Fujitsu Sci. Tech. J*. **2003**, *39*, 40-51.
[30] A. Helwig, G. Müller, G. Sberveglieri, M. Eickhoff, *Journal of Sensors*, **2009**, *Article ID 620720*, 17 pages,
[31] B. Weisz, *J. Chem. Phys*. **1953**, *21,* 1531-1538.
[32] J.J. Velasco-Velez, C. Wilbertz, T. Haas, T. Doll, *Procedia Chemistry*, *2009*, *1*, 642-645
[33] T. Doll, *Advanced Gas Sensing: The Electroadsorptive Effect and Related Techniques*, Kluwer, Boston, 2003
[34] A. Oprea, E. Moretton, N. Bârsan, W.J. Becker, J. Wöllenstein, U. Weimar, *J. Appl. Phys*, **2006**, *100*, 033716-033716-10.
[35] H. Geistlinger, *Surf. Sci*. **1992**, *277*, 429-441.
[36] J.J. Velasco-Vélez, U. Kunze, T. Haas, T. Doll, *Phys. Stat. Sol. A* **2010**, *207*, 924-929.
[37] W. Shockley W.T. Read, *Phys. Rev. Lett*., **1952**, *87,* 835-842.
[38] $E_F = E_F(VG)$. $E_{cs} = 0$ eV (reference energy position), $E_t = 1.1$ eV and $K_n = 10\text{-}13$ m^3/s

Received: ((will be filled in by the editorial staff)) Published online: ((will be filled in by the editorial staff))

Figure 1 enlarged:

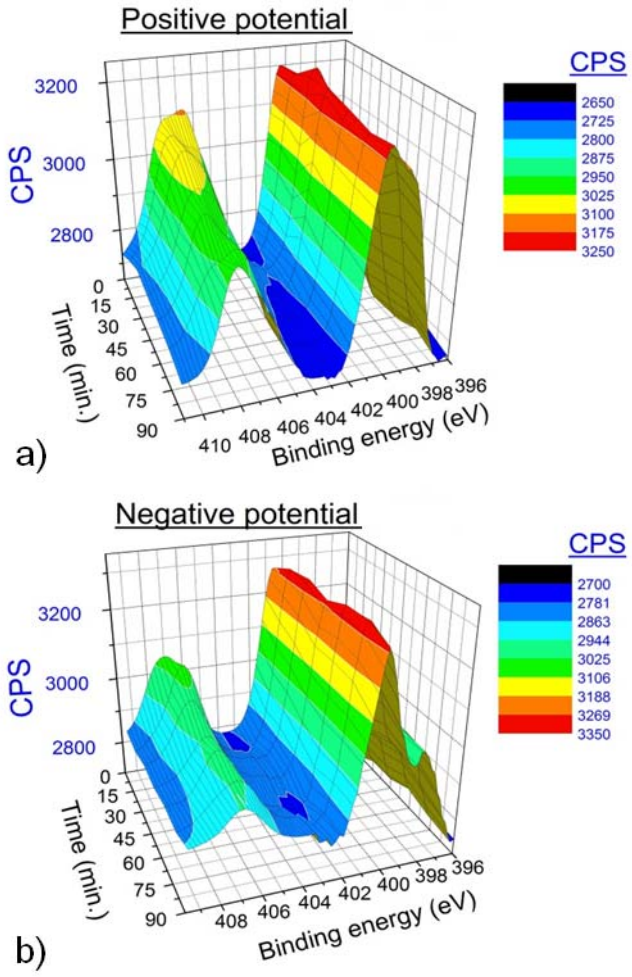

Figure 2 enlarged:

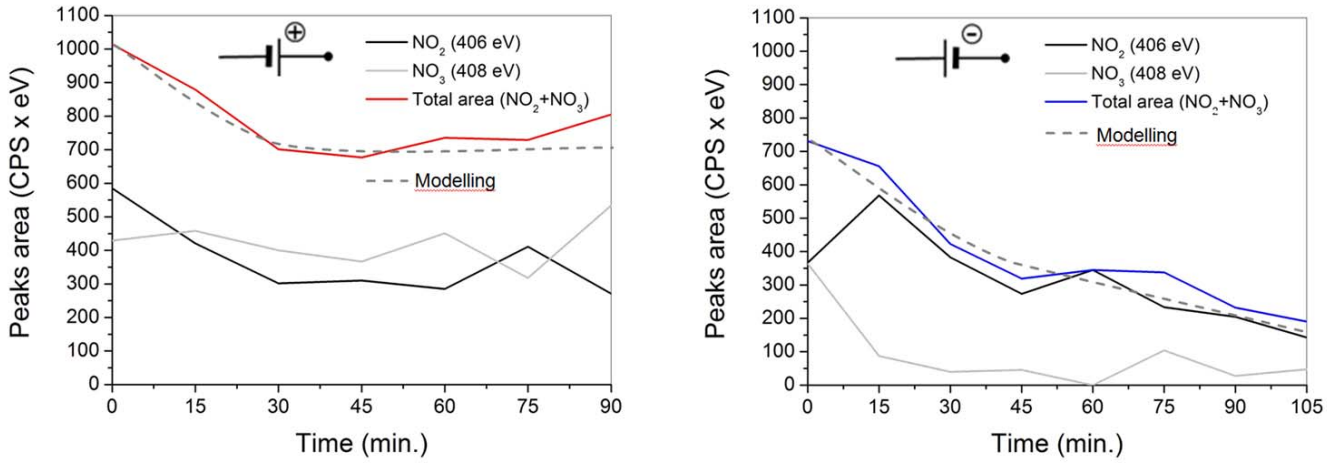

Figure 4 enlarged:

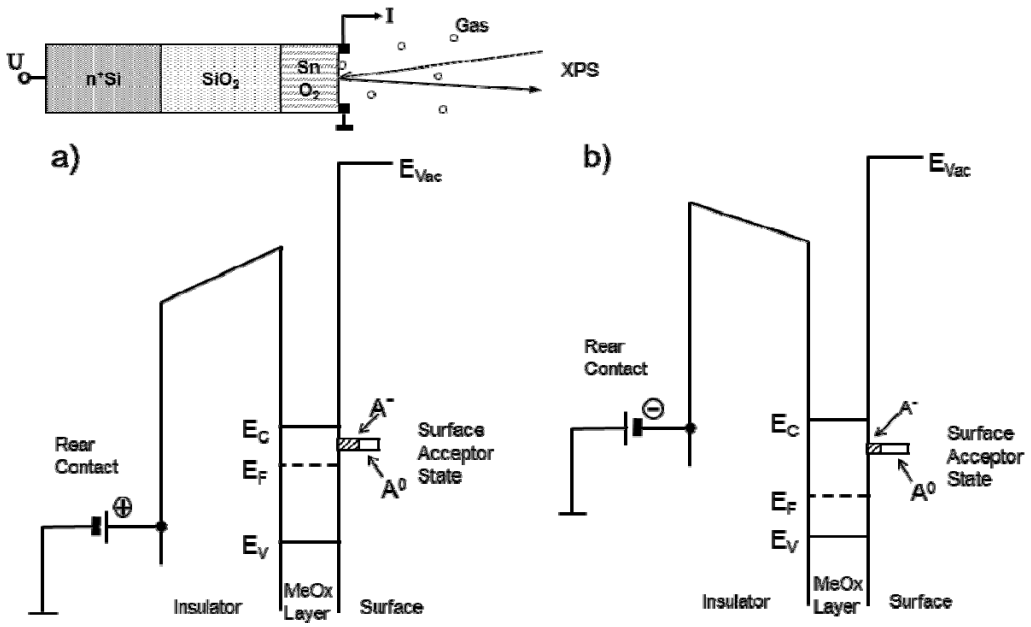

Figure 5 enlarged: